Measurement of ultrafast carrier dynamics in epitaxial graphene

Jahan M. Dawlaty,[a] Shriram Shivaraman, Mvs Chandrashekhar, Farhan Rana, and Michael G. Spencer
School of Electrical and Computer Engineering, Cornell University, Ithaca, New York 14853, USA

(Received 29 November 2007; accepted 28 December 2007; published online 30 January 2008)

Using ultrafast optical pump-probe spectroscopy, we have measured carrier relaxation times in epitaxial graphene layers grown on SiC wafers. We find two distinct time scales associated with the relaxation of nonequilibrium photogenerated carriers. An initial fast relaxation transient in the 70–120 fs range is followed by a slower relaxation process in the 0.4–1.7 ps range. The slower relaxation time is found to be inversely proportional to the degree of crystalline disorder in the graphene layers as measured by Raman spectroscopy. We relate the measured fast and slow time constants to carrier-carrier and carrier-phonon intraband and interband scattering processes in graphene. © *2008 American Institute of Physics*. [DOI: 10.1063/1.2837539]

Graphene is a single two dimensional atomic layer of carbon atoms forming a honeycomb crystal lattice.[1,2] It is a zero-bandgap semiconductor with a linear energy dispersion relation for both electrons and holes.[2] The unusual electronic and optical properties of graphene have generated interest in both experimental and theoretical arenas.[2–4] The high mobility of electrons in graphene has prompted a large number of investigations into graphene based high speed electronic devices, such as field-effect transistors, pn-junction diodes and transistors, and terahertz oscillators.[5–8]

Recently, epitaxial growth of graphene by thermal decomposition of SiC surface at high temperatures has been demonstrated.[4] This technique can provide anywhere from a few monolayers of graphene to several (>50) layers on the surface of a SiC wafer. Graphene layers grown by this technique have demonstrated structural and electronic properties similar to those of graphene layers obtained by micromechanical cleaving techniques.[4,9] The electronic as well phononic properties of epitaxially grown graphene multilayers have been found to be different from those of bulk graphite and similar to those of a graphene monolayer indicating that the electrons and phonons in different layers in epitaxially grown graphene are uncoupled.[10] This observed difference has been attributed to a different stacking scheme for carbon atom layers in epitaxial graphene compared to bulk graphite.[10]

In this paper, we present results from measurements of the ultrafast dynamics of photoexcited carriers in graphene for the first time. Ultrafast studies of carrier dynamics in other forms of carbon, such as carbon nanotubes and bulk graphite, have been reported in the past.[11,12] The results presented in this paper are relevant for understanding carrier intraband and interband scattering mechanisms in graphene and their impact on proposed and demonstrated graphene based electronic and optical devices.[5–8]

The graphene samples used in this work were epitaxially grown on the carbon face of semi-insulating 6*H*-SiC wafers using the techniques that have been previously reported in detail.[12] Samples A, B, and C were grown at temperatures varying from 1400 to 1600 °C and pressures of $(2-7)\times10^{-6}$ torr. Micro-Raman spectroscopy of all samples showed a single-resonant G peak close to 1580 cm^{-1}, a double-resonant D' peak close to 2700 cm^{-1}, and also a relatively low intensity double-resonant D peak near 1350 cm^{-1}.[12] The D peak is not allowed in perfect graphene layers since it requires an elastic scattering process, which is made possible by disorder, to satisfy momentum conservation.[13] The presence of the D peak, therefore, indicates the presence of disorder in the samples. A discussion of the observed intensity of the D peak and its correlation with the measured carrier relaxation times is presented later in this paper. Fourier transform infrared (FTIR) spectroscopy of the samples revealed a flat absorption profile in the 2.5–25 μm range, which is consistent with the massless Dirac-like energy dispersion of electrons and holes. The number of graphene layers in samples A, B, and C were estimated from FTIR and x-ray photoelectron spectroscopies (using the thickogram method[14]) to be 6, 12, and 37, respectively, with less than 5% error.

A Ti:sapphire mode-locked laser with 81 MHz pulse repetition rate, 780 nm center wavelength, and ~85 fs pulse width was used for time-resolved pump-probe spectroscopy of the graphene samples. Pump pulses with energies between 3 and 15 nJ were used to generate photoexcited carriers, while weak probe pulses with energies between 30 and 100 pJ were used to measure the changes in the transmittivity of the samples at various delays of the probe pulses with respect to the pump pulses. The angle of incidence of the pump and probe beams were 0° and 15°, respectively. The pump and the probe were focused to a spot size of about 100 μm. The polarization of the probe was rotated by 90° with respect to the pump, and a polarizer was used to eliminate scattered pump light going in the direction of the probe beam. The probe beam was passed through a 50 μm spatial filter for further removal of the scattered pump light. The pump and probe beams were both modulated at two different frequencies near ~3 KHz, and changes in the intensity of the probe pulses at the sum of these two frequencies were measured with a lockin amplifier.

Photon interband absorption in graphene at optical and near-infrared frequencies is given by the optical conductivity,[8] $\sigma(\omega)=-e^2/4\hbar[f_c(\hbar\omega/2)-f_v(-\hbar\omega/2)]$, where $f_c(E)$ and $f_v(E)$ are the probabilities for the occupation of an energy level with energy E in the conduction and valence bands, respectively. The only frequency dependence of $\sigma(\omega)$

[a]Electronic mail: jd234@cornell.edu.

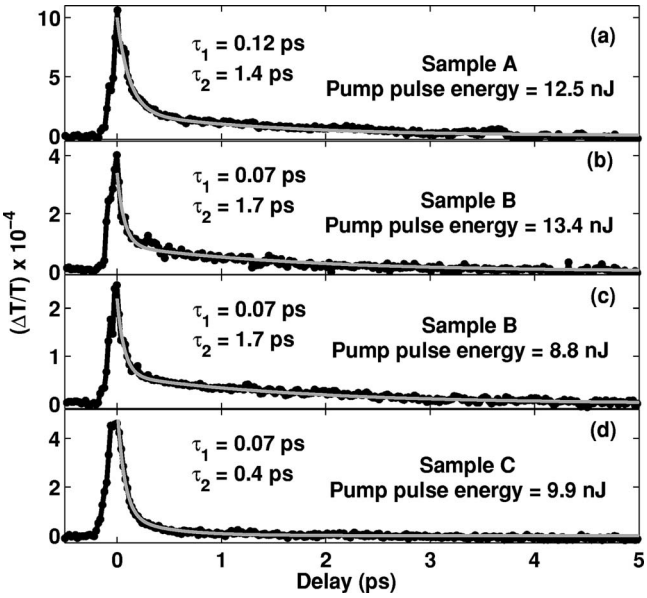

FIG. 1. Measured transmittivity transients for (a) sample A, (b) sample B, (c) sample B with different pump powers, and (d) sample C. The dark solid lines with markers are the experimental data and the light solid lines without markers are analytical fits to the data using exponentials with time constants τ_1 and τ_2. The transients in (b) and (c) show that the slower time constant τ_2 does not change much as the pump energy is varied.

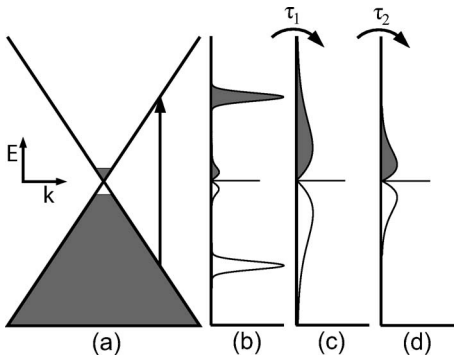

FIG. 2. (a) Band structure of graphene showing an intrinsic population of electrons and holes near the Dirac point. Optical excitation is indicated by the arrow. (b) The nonequilibrium distribution of photoexcited carriers account for the initial rise in transmittivity. (c) The carriers equilibrate among themselves through carrier-carrier scattering on a time scale given by τ_1 resulting in a hot carrier distribution. (d) Subsequent cooling and decay of the hot distribution through carrier-phonon scattering (and possibly electron-hole recombination) occurs on a time scale given by τ_2.

comes from the carrier distribution functions. Matching the optical boundary conditions at the air/graphene/SiC interfaces, the optical transmission $t(\omega)$ through N graphene layers on a SiC wafer (normalized to the transmission through a plain SiC wafer) can be written as

$$t(\omega) = \frac{1}{1 + N\sigma(\omega)\sqrt{\mu_o/\epsilon_o}/(1 + n_{\mathrm{SiC}})}, \quad (1)$$

where n_{SiC} is the refractive index of SiC. The above expression can be used to estimate that pump pulses with energies in the range indicated above generate electron and hole densities in the $3\times10^{11}-10^{12}$ cm^{-2} range. The photogenerated carrier densities are larger than the intrinsic electron and hole densities of $\sim 8\times10^{10}$ cm^{-2} in graphene at room temperature.

Figure 1 shows the transmittivity transients for different graphene samples. The figure shows the time dependent change ΔT in the transmittivity normalized to the transmittivity in the absence of the pump pulse. Transmittivity increases sharply immediately after photoexcitation. The recovery of the transmittivity exhibits two distinct time scales; an initial fast relaxation time τ_1 in the 70–120 fs range, followed by a slower relaxation time τ_2 in the 0.4–1.7 ps range. These time constants have been extracted by analytical fits to the data using decaying exponentials. It should be noted here that the faster time τ_1 is of the order of the pulse width and is, therefore, not accurately resolvable.

A simple model incorporating band-filling effects together with intraband carrier-carrier and carrier-phonon scattering can be used to explain the observed transmittivity transients. Figure 2 is a schematic representation of this model. Photogeneration of carriers by the pump pulse reduces the number of empty conduction band and filled valence band states and causes the initial increase in the transmittivity observed in Fig. 1. Immediately after photoexcitation, the nonequilibrium carrier distribution broadens and also equilibrates with the intrinsic carrier population through carrier-carrier scattering. This process results in the initial fast relaxation of the transmittivity. The observed fast relaxation times (τ_1) are consistent with the theoretically predicted carrier-carrier intraband scattering rates in graphene in Ref. 15. As a result of carrier-carrier scattering the photogenerated carriers are expected to equilibrate among themselves and reach a Fermi–Dirac-like distribution with a temperature much higher than the lattice temperature. The slower time constant (τ_2) of the transmittivity decay could be attributed to the subsequent thermalization of the carriers with the lattice through carrier-phonon intraband scattering.

Electron-hole recombination processes could also contribute to the slow decay of the transmittivity. The dominant mechanisms for electron-hole recombination in graphene are not yet well understood. In Ref. 16, electron-hole recombination due to Auger scattering in graphene was analyzed and carrier density dependent lifetimes of the order of a few picoseconds for electron-hole densities in the $10^{11}-10^{22}$ cm^{-2} range were predicted. However, varying the pump pulse energies in the 3–15 nJ range to vary the photogenerated carrier densities did not lead to any significant changes in the values of τ_2. For example, Figs. 1(b) and 1(c) show the transmittivity transients for two different pump pulse energies for sample B. These results indicate that the dominant contribution to τ_2 comes from a process that is independent of the carrier density and is likely carrier-phonon rather than carrier-carrier scattering. However, electron-hole recombination due to carrier-phonon interband scattering cannot be ruled out. It needs to be pointed out here that carrier-phonon scattering cannot be ruled out as a contributor to the fast relaxation time τ_1 from our measurement results.

It has been shown that carrier-phonon deformation potential scattering rates in semiconductor nanostructures are enhanced in the presence of disorder.[17] In graphene, the intensity of the double-resonant D peak (near 1350 cm^{-1}) in the Raman spectrum can be used as a measure of crystalline disorder since this peak is absent in perfect graphene layers.[13] The ratio of the intensities, I_G and I_D, of the G and D peaks, respectively, in the Raman spectrum has been shown to be proportional to the crystal coherence length.[18] Thus, one could expect the time constant τ_2 to scale with the

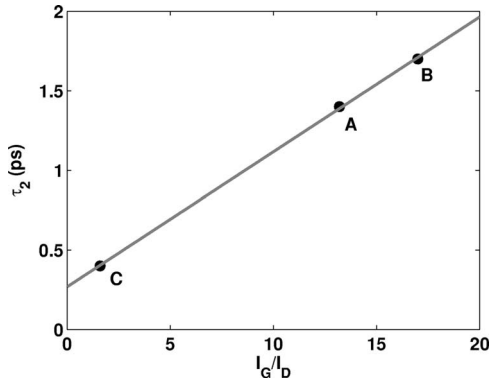

FIG. 3. The slower relaxation time τ_2 is plotted vs the ratio of the intensity of the Raman *G* and *D* peaks for samples A, B, and C. This ratio is a measure of the crystal coherence length. Larger crystal disorder (smaller coherence length) results in shorter relaxation times.

ratio I_G/I_D. Figure 3 shows the values of τ_2 plotted versus the ratio I_G/I_D for the three samples. Figure 3 shows that $\tau_2 \propto I_G/I_D$ and, therefore, τ_2 is proportional to the coherence length of the crystal. These results also support electron-phonon scattering as the dominant mechanism contributing to τ_2.

Figure 4 shows the peak value (normalized) of the transmittivity change $\Delta T/T$ plotted as a function of the pump pulse energy for sample B. As expected from linear absorption and final state filling arguments, the maximum value of $\Delta T/T$ is proportional to the pump pulse energy. These data also rule out any significant role played by nonlinear two-photon pump absorption in the transmittivity transients. Complete saturation or bleaching of the absorption is not observed for the range of pump pulse energies used in the experiments. From the density of states of graphene, it follows that the maximum electron density in an energy interval ΔE centered at E is $2E\Delta E/\pi\hbar^2 v^2$, where v is the velocity of carriers in graphene and is equal to 10^8 cm/s.[2] Setting $E=\hbar\omega/2$ and $\Delta E=\hbar\Delta\omega/2$, where $\Delta\omega$ is the optical bandwidth of the pump pulse ($\sim$10 nm), the maximum electron (or hole) density comes out to be 1.1×10^{12} cm^{-2} for 780 nm pump center wavelength. The fact that no bleaching of the absorption is observed even for pulse energies large enough to excite electron (and hole) densities close to 10^{12} cm^{-2} is

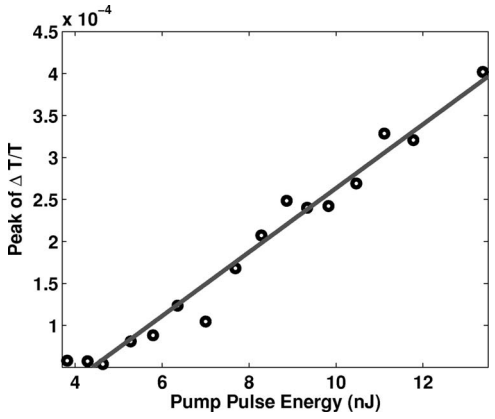

FIG. 4. Peak transmittivity after photoexcitation is plotted for various pump energies for sample B. Linear relation between the transmittivity peak and the the pump pulse energy agrees with the linear absorption and band filling model.

because of the fast relaxation time τ_1, which is of the order of the pump pulse width. Therefore, Graphene has potential use as a fast saturable absorber for generating high energy short pulses from modelocked lasers.[18]

In conclusion, we have measured ultrafast carrier relaxation rates in epitaxially grown graphene layers on SiC.[11,12] Our measurements indicate the separate roles played by carrier-carrier and carrier-phonon scattering in relaxing photogenerated carriers.

More work is needed to investigate the role of carrier-phonon scattering in the fast relaxation time τ_1, the role of electron-hole recombination in the slow relaxation time τ_2, and the value of τ_2 in the limit of disorder-free epitaxial graphene layers. It has been recently pointed out that the first few carbon layers in epitaxially grown graphene acquire a bandgap as a result of interaction with the atoms in the SiC substrate.[19] The effect of bandgap on ultrafast intraband and interband carrier dynamics is not clear. More experiments with fewer monolayers of epitaxial graphene would be needed to explore the effects of bandgap on carrier dynamics.

The authors acknowledge support from the National Science Foundation, the Air Force Office of Scientific Research under Contract No. FA9550-07-1-0332 (contract monitor Dr. Donald Silversmith), and Cornell Material Science and Engineering Center (CCMR) program of the National Science Foundation (Cooperative Agreement No. 0520404).

[1] R. Saito, G. Dresselhaus, and M. S. Dresselhaus, *Physical Properties of Carbon Nanotubes* (Imperial College Press, London, UK, 1999).
[2] K. S. Novoselov, A. K. Geim, S. V. Morozov, D. Jiang, M. I. Katsnelson, I. V. Grigorieva, and S. V. Dubonos, A. A. Firsov, Nature (London) **438**, 197 (2005).
[3] Y. Zhang, Y. Tan, H. L. Stormer, and P. Kim, Nature (London) **438**, 201 (2005).
[4] C. Berger, Z. Song, X. Li, X. Wu, N. Brown, C. Naud, D. Mayou, T. Li, J. Hass, A. N. Marchenkov, E. H. Conrad, P. N. First, and W. A. de Heer, Science **312**, 1191 (2006).
[5] G. Liang, N. Neophytou, D. E. Nikonov, and M. S. Lundstrom, IEEE Trans. Electron Devices **54**, 657 (2007).
[6] J. R. Williams, L. DiCarlo, and C. M. Marcus, Science **317**, 638 (2007).
[7] G. Gu, S. Nie, R. M. Feenstra, R. P. Devaty, W. J. Choyke, W. K. Chan, and M. G. Kane, Appl. Phys. Lett. **90**, 253507 (2007).
[8] F. Rana, IEEE Trans. Nanotechnol. **7**, 91 (2008); Also available at e-print arXiv:cond-mat/0710.3556.
[9] T. Ohta, A. Bostwick, T. Seyller, K. Horn, and E. Rotenberg, Science **313**, 951 (2006).
[10] J. Hass, F. Varchon, J. E. Millan-Otoya, M. Sprinkle, W. A. de Heer, C. Berger, P. N. First, L. Magaud, and E. H. Conrad, e-print arXiv:cond-mat/0706.2134.
[11] Y. Ma, J. Stenger, J. Zimmermann, S. M. Bachilo, R. E. Smalley, R. B. Weisman, and G. R. Fleming, J. Chem. Phys. **120**, 3368 (2004).
[12] K. Seibert, G. C. Cho, W. Kütt, H. Kurz, D. H. Reitze, J. I. Dadap, H. Ahn, M. C. Downer, and A. M. Malvezzi, Phys. Rev. B **42**, 2842 (1990).
[13] A. C. Ferrari and J. Robertson, Phys. Rev. B **61**, 14095 (2000).
[14] P. J. Cumpson, Surf. Interface Anal. **29**, 403 (2000).
[15] E. H. Hwang, B. Y. Hu, and S. Das Sarma, Phys. Rev. B **76**, 115434 (2007).
[16] F. Rana, Phys. Rev. B **76**, 155431 (2007).
[17] A. Sergeev, M. Yu. Reizer, and V. Mitin, Phys. Rev. Lett. **94**, 136602 (2005).
[18] F. X. Kartner, J. A. der Au, and U. Keller, IEEE J. Sel. Top. Quantum Electron. **4**, 159 (1998).
[19] S. Y. Zhou, G. H. Gweon, A. V. Fedorov, P. N. First, W. A. de Heer, D. H. Lee, F. Guinea, A. H. Castro Neto, and A. Lanzara, Nat. Mater. **6**, 770 (2007).